KW

Met O 11

Technical Note No. 226

A study of the structure of mid-latitude depressions in a numerical model using trajectory techniques. II: Case Studies

by

B. Golding

Meteorological Office, Met O 11

London Road

Bracknell

Berkshire

England

A study of the structure of mid-latitude depressions in a numerical model using trajectory techniques. II: Case Studies

By B. Golding

Meteorological Office, Bracknell

SUMMARY

The diagnostic techniques developed in Part I are used to investigate the airflow structure of real depressions. Attention is concentrated on a vigorous system which passed near the British Isles on 12/9/1979. Some similarities and differences are found between the patterns of temperature, vorticity and vertical velocity in this system when compared to the ideal baroclinic wave. The relative motion air trajectories are shown to be very like those found in Part I except for a feature of the warm front outflow which can be explained in terms of the more vigorous uplift in the present case. Summaries of seven other cases are presented which support the thesis that these qualitative air flow characteristics are a normal feature of baroclinic systems in the atmosphere.

1. INTRODUCTION

The work described in this paper forms the second part of an attempt to relate the observed features of mid-latitude depressions to the theory of baroclinic wave development. In the first part (Golding 1984, hereafter referred to as G) the structure of ideal baroclinic waves was investigated. Simulations of baroclinic wave development in dry and moist atmospheres were performed using the UK Meteorological Office 10-level model (Burridge & Gadd 1977, Gadd 1978a, b, 1980). The results were portrayed in terms of diagnostic maps and air parcel

trajectories. Both were compared with similar diagnostics obtained from integrations of the semi-geostrophic equations by Hoskins and West (1979). Reasonable agreement was found and reasons for the discrepancies were suggested. The trajectory results were summarised into a series of conceptual diagrams for air flow near 950 mb and 750 mb which are reproduced in Fig 1. Three phases were identified: a linear stage in which the structure resembles that of a normal mode disturbance and the low level flow is everywhere slower than the system propagation speed (panels a, b); a mature stage in which the warm air flow on the south side of the pressure centre is faster than the system propagation speed, leading to the development of flow separation zones marked with the appropriate frontal symbols (panels c, d); and an occluded stage in which the cold air circulates round the centre of the system and the cold front consequently takes on changed characteristics. In a moist atmosphere, the flow regimes developed in a similar way but with much more intensity. The locally reduced stability led to development of secondary circulations near the fronts and to a narrowing of the warm air flow ahead of the cold front.

In this second part, some real atmospheric systems are investigated in a similar manner to identify the aspects of their flow structure which are related to those described in G. In this way the extensive theoretical investigations of baroclinic wave development referred to in G may be related a little more closely to the depressions which are observed in the atmosphere. To do this, the forecast from midnight on 12/9/1979 will be described in some detail

using the techniques described in G. Several other cases will then be presented in outline. Fuller descriptions of these cases can be found in Golding (1981).

Investigation of these real disturbances requires some changes to the modelling approach. Their smaller scale is accommodated by using the fine mesh, 100 km resolution, version of the 10-level model. This covers a smaller domain than the almost hemispheric 300 km resolution version used in G. However, for simplicity and in view of the short duration of the simulations (24 hours), the boundary values were still kept fixed. Some resulting distortions late in the forecast period will be noted in the results. In addition, in order to keep as close as possible to the observed development, the full suite of parametrizations was retained in the model. There included a radiation scheme with model determined cloud layers, a surface exchange scheme with surface heat balance and bulk mixing terms, and a deep convection parametrization. In the dry integration presented for comparison in section 2, the initial humidity values were set to zero everywhere but the full set of parametrizations was still retained leading undoubtedly to a slow moistening of the model from the surface upwards. As will be seen, however, the air parcel trajectories show clearly the effect of the initial dryness. The techniques for computing the trajectories are essentially the same as in G except that model output is available every 10 mins and so parcel positions are computed every 20 mins. To simplify the diagrams, however, the crosses depicting parcel altitude are plotted every 3rd location i.e. every hour.

3. CASE STUDY

The case chosen for full presentation is a vigorous depression which developed to the northwest of Britain on 12/9/1979. It formed as a cold front wave disturbance in the western Atlantic and deepened steadily as it moved east. During the period of analysis it deepened rapidly taking a north eastward track close to northwest Scotland. The surface frontal analysis for midday is shown in Fig. 2. It shows a mature system with well developed fronts which are beginning to occlude. A marked ridge has developed ahead of the system but the analyst has retained the frontal connection with the downstream system. The satellite photographs, Figs. 3,4, show the system in the early afternoon, a little later than in Fig. 2. The visible picture (Fig. 3) shows a well marked mass of cloud associated with the depression. There is a narrow band of cloud along the cold front which broadens into an extensive shield ahead of the warm front and the centre. At its western end it can be seen curling round the vortex. The infrared picture (Fig. 4) shows that most of the cold front cloud and that curling round the centre is at fairly low levels. Cirrus is observed as a narrow part of the cold front band over Northern Ireland. From there it broadens out to form the northern part of the warm front shield. A further band of slightly lower cloud appears to curve left in the region of the analysed triple point. These structural features in the cloud field are suggestive of air motion but it should be noted that they cannot represent trajectories because of the rapid evolution of the system.

The forecast was run from midnight initial data and Figs. 5-10 show the diagnostic fields for midday. The 1000 mb height field (Fig 5) has its centre close to that in Fig. 2 but with a much overestimated surface pressure. Indeed the predicted deepening over 12 hours was 9 mb, about half that observed. Figure 6 shows the predicted 500 mb field with a trough near 15°W, some 5° west of the surface centre. The trough is confluent with a well market jet maximum above the surface system. The 1000 mb relative vorticity pattern is shown in Fig. 7. A region of large cyclonic vorticity is centred on the surface pressure centre with a peak value of 1.8 x $10^{-4}s^{-1}$ and extends southward along the cold front with values of 5 x $10^{-5}s^{-1}$ as far south as 47°N. Much smaller values are found in the warm front region east of the centre, though a minor peak of 5 x $10^{-5}s^{-1}$ is located in the northeast corner of Scotland. Figure 8 shows the 550 mb vertical velocity field. A large area of ascent lies ahead of the surface warm front position with peak values of 7 μbs^{-1} over the centre and 4 μbs^{-1} at its eastern extremity. There is only weak ascent in the cold front region, indistinguishable from that over the whole of the warm sector region. The low level temperature structure (Fig. 9) shows that the model has a rather weak gradient in the frontal regions. Nevertheless the 5° isotherm interval clearly marks their general locations. Finally Fig. 10 shows a composite of the main features of these diagnostic maps. A comparison with day 5 of the ideal run in Fig 7 of G shows that the spatial relationship between the fatures is largely retained but that the vorticity is more concentrated on the cold front and gradients are generally much larger.

In order to investigate the airflow through the system, trajectories were computed for a set of air parcels which at midnight formed a square grid with 200 km spacing around the centre of the depression. Parcels were initiated at 750 mb and 950 mb. In order to simplify the presentation, only a small number of selected trajectories is presented in each diagram, and a schematic interpretation is given alongside. In all diagrams flow relative to the movement of the pressure centre is shown. The trajectory plots indicate increasing altitude by increasing cross size and vice versa. The arrows in the schematics thicken towards the head for ascent and vice versa. Figures 11, 12 show the flow deduced from the trajectories initiated at 950 mb. The centre of the vortex is clear and a marked separation can be traced to the south of this between southward flowing cold air parcels on the left and northward flowing warm air parcels on the right. This is comparable with Fig. 10 in G where the feature was identified with the synoptically defined cold front. Here that identification can be confirmed by reference to the analysis in Fig. 2. This flow separation is characterised mainly by horizontal shear although some uplift occurs in the trajectories to the right. To the right of the vortex centre, the northward moving parcel trajectories show a dramatic increase in altitude over a short distance, overlaying westward travelling parcels at low levels. Again this is in agreement with Fig. 10 of G but the magnitude of the ascent is much greater. At the eastern end, some parcels reach above the local steering level to turn rightwards away from the centre. However, as in the ideal runs, most parcels turn left to spiral round the vortex. Two trajectories are marked in Fig. 11 for further study.

Diagnostics along their length are shown in Fig. 13. Both parcels are in the warm airflow which rises over the warm front, the first (labelled a) turning cyclonically into the vortex, and the other (labelled b) turning anticyclonically into the upper jet. The first ascends throughout the 24 hour period reaching a peak rate of $9\mu bs^{-1}$ at about 10 hours. This is a little before the time when its relative direction of motion turns from northward to westward. The exact time of the turning coincides with the peak in the vorticity and deformation curves at 11 hours. The peak value of vorticity is $1.7 \times 10^{-4}s^{-1}$. The divergence curve is closely correlated with the vorticity changes as would be expected in a region of strong vorticity generation by stretching. In the 24 hours this parcel rises nearly 400 mb reaching 560 mb at the end. This can be compared with a 300 mb rise in 48 hours for a comparably situated parcel in the ideal run. The temperature profile closely follows the saturated adiabat, indicating the role of moisture in generating the uplift. The parcel marked b also ascends throughout the period but the curves have been stopped at 19 hours after which some boundary distortion became evident. A peak vertical velocity of $6\mu bs^{-1}$ is shown at 17 hours. This parcel has a much lower initial vorticity which increases during ascent. It is well correlated with the divergence curve. The overall ascent is 200 mb and the temperature curve is slightly below the saturated curve, presumably due to mixing.

Figure 14 shows a selection of trajectories initiated at 750 mb and they are interpreted in Fig. 15. The western cyclonic vortex marks the low pressure centre at this level while the eastern, anticyclonic one appears in the relative flow framework where the

inflow from the east at about 750 mb is processed in the system and reappears travelling eastwards at high levels. As in the ideal run there is only weak evidence for a flow separation to the south of the centre. Two trajectories are labelled in Fig. 14 for further study in Fig. 16. One stays near the vortex throughout the period (a) and the other moves rapidly away to the east after ascending in the warm front(b). Both suffer from proximity to the northern boundary at the end and have been cut short where this becomes evident. Parcel 'a' sustains high vertical velocities of 11-12μbs^{-1} for a long period taking it up to 380 mb by the end. The vorticity also starts high, reaching a maximum of $1.6 \times 10^{-4} s^{-1}$ before decreasing. The divergence is small throughout and shows no correlation with the vorticity profile. The temperature drop is steep but consistent with saturated adiabatic ascent. Indeed the simulated temperature and pressure changes indicate the loss of over 90% of the initial $9gkg^{-1}$ water content. Parcel 'b' also shows large values of vertical velocity and vorticity. However both fall to small values after 12 hours as it turns to the right. The maximum rate of ascent is $14\mu bs^{-1}$ between 4-8 hours and this parcel reaches 350 mb by the end of the diagnostics, a rise of 400 mb in 16 hours. The temperature drop again follows the saturated adiabat. The general behaviour of these parcels agrees with those in fig 16 of G for the ideal moist run. However amplitudes are very much greater here.

A major interest in G was the effect of moisture on the development of the baroclinic wave. Here, the same problem is looked at in reverse by removing moisture from the simulation. Two diagnostic fields serve to illustrate the effect of doing this.

Figure 17 shows the 1000 mb height field for midday for comparison with Fig. 5. The 12 hour deepening of the centre has been reduced from 9 mb to 5 mb. This is consistent with the results obtained in G where, for the mature phase, the rate of deepening was doubled in a saturated atmosphere. This is despite the fact that the system has a memory, in its initial conditions, of the effect of moisture in getting it to that stage. Figure 18 shows the 550 mb vertical velocity field with maximum ascent of $4\mu bs^{-1}$ over the centre compared with $7\ \mu bs^{-1}$ in Fig. 8. Ascent over the warm front has all but gone. The 950 mb trajectories show the same basic structure as before but with very small vertical displacements. Consequently, the warm air parcels all turn left at the warm front. Figure 19 shows the diagnostic profiles for parcel 'a' of Fig. 11 in the dry run. This confirms the weakness of the vertical motion. The vorticity is comparable with that in Fig. 13 illustrating the system's memory of its initial conditions. Thus, while the developmental diagnostics are affected by dryness in the same way as in the ideal run, the effect of the initial conditions makes the two dimensional structure retain the characteristics of a moist system.

3. CASE SUMMARIES

Each case in this section will be illustrated by two diagrams: the surface frontal analysis and a schematic diagram of the relative air flow of parcels originating at 950 mb over a 24 hour period. To facilitate comparison, the conceptual diagrams have been rotated so that the direction of system motion is to the right.

Figure 20 shows an intense depression with well occluded fronts and a circulation covering much of the North Atlantic. It is analysed with a secondary cold front occupying a trough to the south of the centre. The simulated flow structure is a little different with the warm front meeting the reaward cold front at the centre. The forward cold front shows both horizontal shear and vertical motion. The warm front shows a similar structure to the ideal run, not having the bifurcation of flow found in section 2.

Figure 21 is another old, slow moving, system in the Atlantic but this time it is the wave on the cold front northwest of Ireland that is of interest. The pre-existence of the frontal boundary must make the early stages of development somewhat different from the ideal run. However the analysed flow structure is very similar to the mature stage there. The cold front shows a pronounced flow reversal while the warm front is characterised by uplift and a leftward turn.

Figure 22 shows a weak system at 46°N 15°W, running down the western flank of a major upper trough. The analyst has interpreted the trailing cloud band as an occluded front and attempted to insert a wave depression structure on the forward side. The simulated flow structure is clearly rather different, having only two flow separation zones. Indeed it is very similar to Fig. 21. The forward zone has a warm front structure with uplift and leftward turning while the trailing one has the same structure as the cold front with a horizontal flow reversal.

Figure 23 shows a pair of vigorous, well occluded systems travelling northwards on the eastern side of a major upper trough. The flow structure is depicted for the northern system. Its occluded

nature is lost in the identification of flow separation zones in the simulation. This leaves a flow structure very similar to those seen before with a horizontal flow reversal at the cold front and upward left-turning flow at the warm front.

Figure 24 shows a small rapidly developing centre which gave rise to the Fastnet storm. This also shows the characteristic air flow pattern despite its small size.

Figure 25 is a quite different type of development. The frontal wave analysed over Ireland developed and subsequently amalgamated with the pre-existing depression to the northwest. The model diagnostics indicate that development was almost entirely on the wave while the old system provided the structure of a deep vortex. The flow pattern does not show the separate components and is close to the ideal pattern.

Finally, Fig. 26 shows another very different system. The depression over England originated as a heat low over France moving slowly north with an associated belt of heavy, thundery rain. At this level, the flow structure does not provide evidence for separation at the warm front although for parcels from 750 mb that evidence is clear. At that level, by contrast, the cold front loses its identity. This combination was observed in the ideal run during the transition from the linear to mature phases.

4. CONCLUSIONS

A detailed case study and the examination of results from 7 other cases has demonstrated that numerical simulations of frontal depressions produce common features in the flow pattern which were also present in the idealised baroclinic wave integrations described

in G. Most of the cases presented here conformed to the mature stage of development illustrated in Fig. 1(c,d). With one exception flow separation zones were identified both ahead of and behind the warm air sector of the system. The forward zone was characterised by uplift over the low level cold inflow and then a sharp turning which at low levels was to the left, into the vortex, and at higher levels was into the upper jet away to the right. Individual cases showed differences in these features due to the strength of the uplift and the size of the upper vortex. The rearward separation zone was usually characterised by a reversal of horizontal flow direction, it being towards the warm front in the warm air. The vertical motion in this region varied considerably between different cases. The diverse systems in which these flow regimes have been identified suggests that they are characteristic of baroclinic eddies regardless of their mode of formation. This structure agrees in many respects with that deduced from observational evidence by Carlson (1980). However, it differs in the origin of the air which circulates round the centre of the system. This difference may reflect deficiencies in the model simulation or in the observational coverage.

The case study comparison of dry and moist integrations confirms the findings of the ideal integrations that the role of latent heat release in the frontal rain areas is critical in determining the rate of development of the system.

Detailed aspects of the simulations have not been presented in this study. Clearly, each had its own peculiar features. However, such detail is more likely to be distorted by the imperfection of the modelling techniques or of the initial state than are the common

features. In this study the circulation in the lower troposphere has been emphasised. The techniques used are also applicable to higher levels and it is hoped that future work in this area may provide a description of the interaction between the warm air outflow and the upper jet.

ACKNOWLEDGEMENTS

The work described in this paper was presented as part of a doctoral thesis of Reading University. I am grateful to my supervisors Prof R P Pearce and Dr A J Gadd for their guidance and support throughout the course of the work. I am also grateful to Prof. B. Hoskins, Mr A Gilchrist, Dr K. Browning and Dr M. Cullen for discussion of the results.

REFERENCES

Burridge, D.M. and Gadd, A.J. 1977 'The Meteorological Office operational 10-level numerical weather prediction model (December 1975)'. Sci. Pap. Met O. No. 34, HMSO.

Carlson, T.N. 1980 Airflow through midlatitude cyclones and the comma cloud pattern. Mon. Wea. Rev. 108, 1498-1509.

Gadd, A.J. 1978a A split explicit integration scheme for numerical weather prediction. Quart. J.R. Met. Soc. 104, 569-582.

1978b A numerical advection scheme with small phase errors. ibid. 104, 583-594.

1980 Two refinements of the split explicit integration scheme. ibid., 106, 215-220.

Golding, B.W. 1981 'Diagnostic studies of mid-latitude depressions'. Ph.D. Thesis, University of Reading.

1984 A study of the structure of mid-latitude depressions in a numerical model using trajectory techniques. I: Development of ideal baroclinic waves in dry and moist atmospheres. Quart. J.R. Met. Soc. 110, 847-879.

Hoskins, B.J. and West, N.V. 1979 Baroclinic waves and frontogenesis. Part II: Uniform potential vorticity jet flows - cold and warm fronts. J. Atmos. Sci. 36 1663-1680.

FIGURES

Fig. 1. Summary of the development of relative air flow in a dry idealised baroclinic wave (from G) Linear Stage. (a - 950 mb, b - 750 mb); Mature stage (c - 950 mb, d - 750 mb); Occluding stage (e - 950 mb, f - 750 mb).

Fig. 2. Surface synoptic analysis for 1200 GMT 12/9/1979.

Fig. 3. Visible satellite picture for 1339 GMT 12/9/1979 from Tiros-N. Courtesy of the University of Dundee electronics laboratory.

Fig. 4. Infra red satellite picture for 1339 GMT 12/9/1979 from Tiros-N. Courtesy of the University of Dundee electronics laboratory.

Fig. 5. Forecast 1000 mb height field for 1200 GMT 12/9/1979 (gpm).

Fig. 6. Forecast 500 mb height field for 1200 GMT 12/9/1979 (gpm).

Fig. 7. Forecast 1000 mb relative vorticity field for 1200 GMT 12/9/1979 ($s^{-1} \times 10^5$).

Fig. 8. Forecast 550 mb vertical velocity field for 1200 GMT 12/9/1979 (μbs^{-1}).

Fig. 9. Forecast 900-1000 mb layer mean temperature field for 1200 GMT 12/9/1979 (K).

Fig. 10. Composite of the low level diagnostic fields for 1200 GMT 12/9/1979.

Fig. 11. Diagnosed trajectories for parcels initially at 950 mb. Increasing altitude is denoted by increasing cross size and vice versa. The axes are numbered in increments of 100 km relative to the model's origin.

Fig. 12. Schematic interpretation of the flow shown in Fig. 11. Ascent is indicated by increasing arrow width towards the head and vice versa.

Fig. 13. Profiles of diagnostic quantities following parcels a, b in Fig. 11.

Fig. 14. Diagnosed trajectories for parcels initially at 750 mb. Increasing altitude is denoted by increasing cross size and vice versa.

Fig. 15. Schematic interpretation of the flow shown in Fig. 14. Ascent is indicated by increasing arrow width towards the head, and vice versa.

Fig. 16. Profiles of diagnostic quantities following parcels a, b in Fig. 14.

Fig. 17. Forecast 1000 mb height field for 1200 GMT 12/9/1979 (gpm). Dry case (cf Fig. 5)

Fig. 18. Forecast 550 mb vertical velocity field for 1200 GMT 12/9/1979 (μbs^{-1}). Dry case (cf Fig. 8).

Fig. 19. Profiles of diagnostic quantities following parcel a in Fig 11. Dry case (cf Fig. 13).

Fig. 20. Surface analysis for 0600 GMT 30/10/1979 and schematic low level trajectory analysis for the following 24 hours.

Fig. 21. surface analysis for 0001 GMT 5/9/1979 and schematic low level trajectory analysis for the 24 hours from 1200 GMT the previous day.

Fig. 22. Surface analysis for 0001 GMT 11/10/1979 and schematic low level trajectory analysis for the previous 24 hours.

Fig. 23. surface analysis for 0001 GMT 21/10/1979 and schematic low level trajectory analysis for the previous 24 hours.

Fig. 24. Surface analysis for 0001 GMT 14/8/1979 and schematic low level trajectory analysis for the 24 hours from 1200 GMT the previous day.

Fig. 25. Surface analysis for 1200 GMT 26/9/1979 and schematic low level trajectory analysis for the 24 hours from 0001 GMT.

Fig. 26. Surface analysis for 1200 GMT 14/6/1980 and schematic low level trajectory analysis for the 24 hours from 0001 GMT.

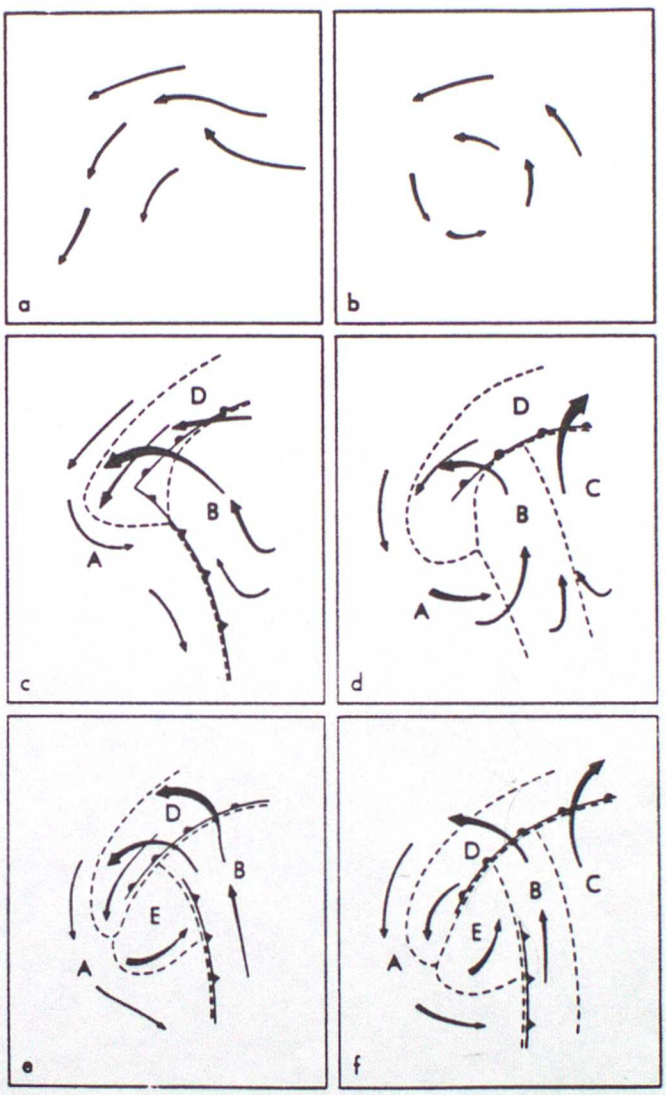

Fig. 1

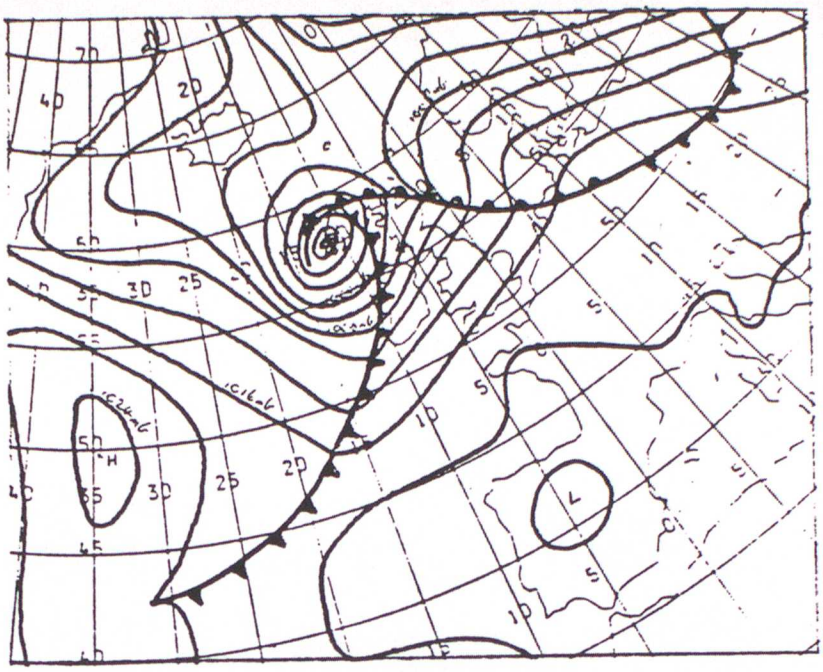

Fig. 2

Fig. 3

Fig. 4

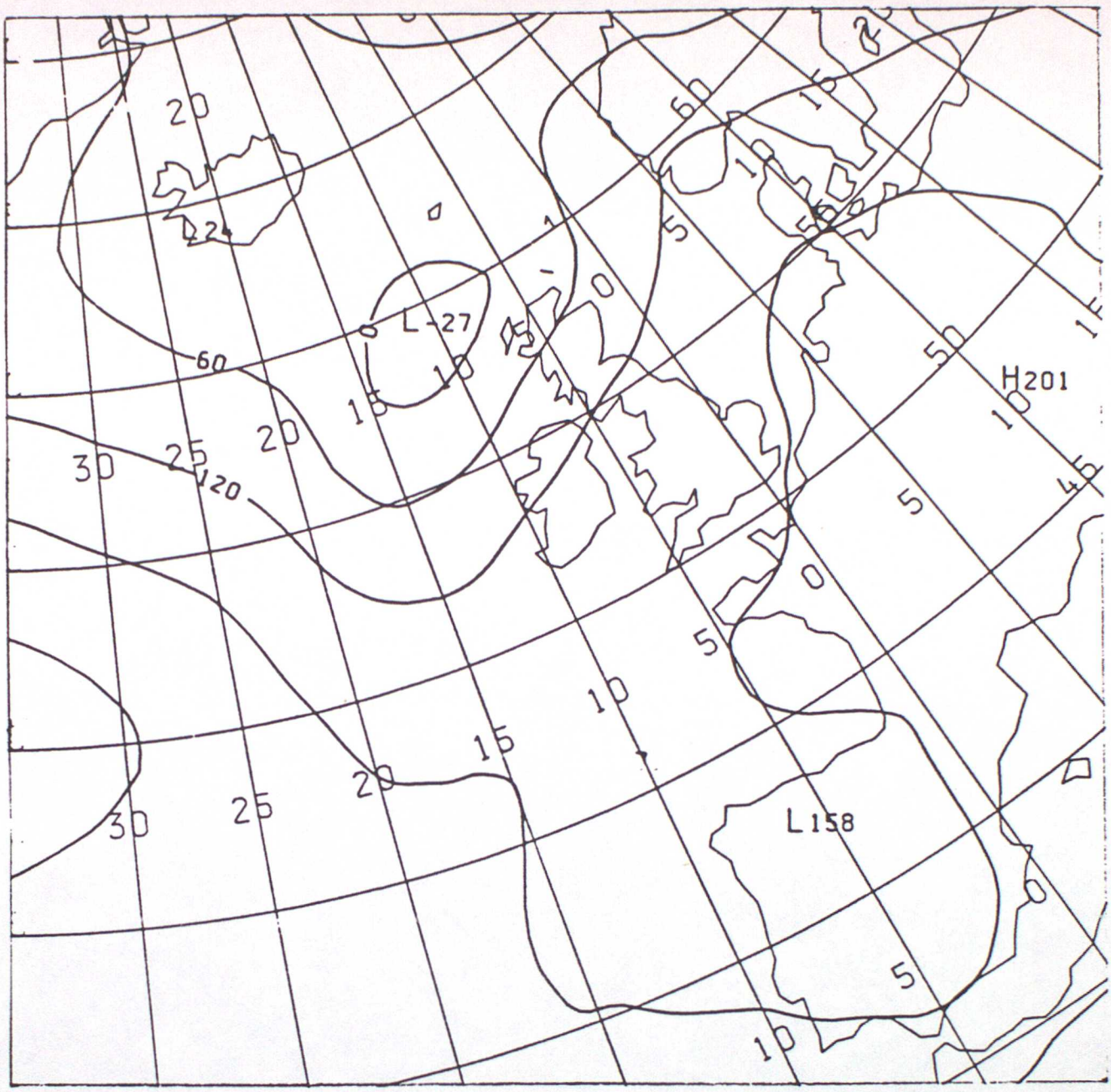

Fig. 5

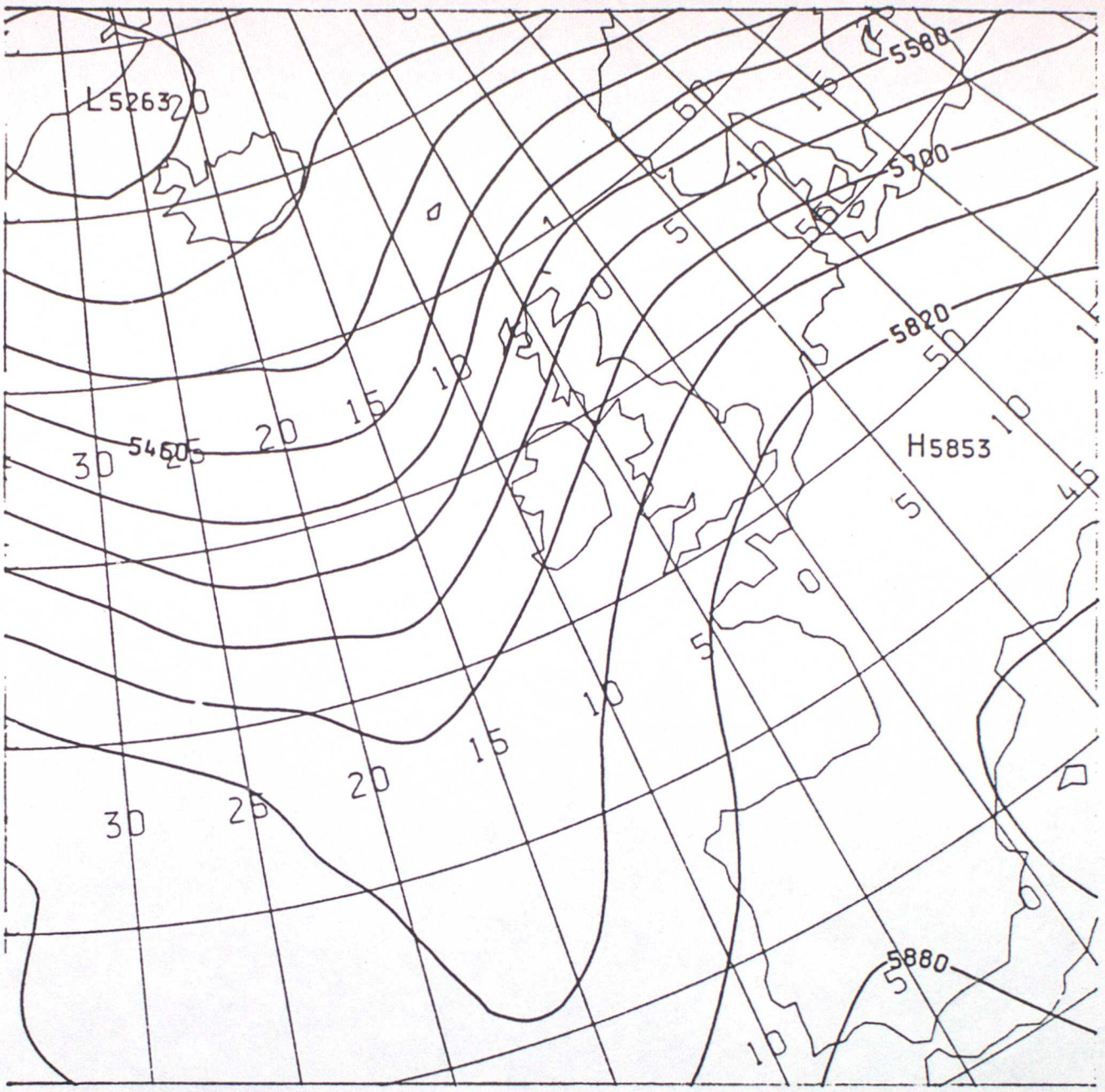

Fig. 6

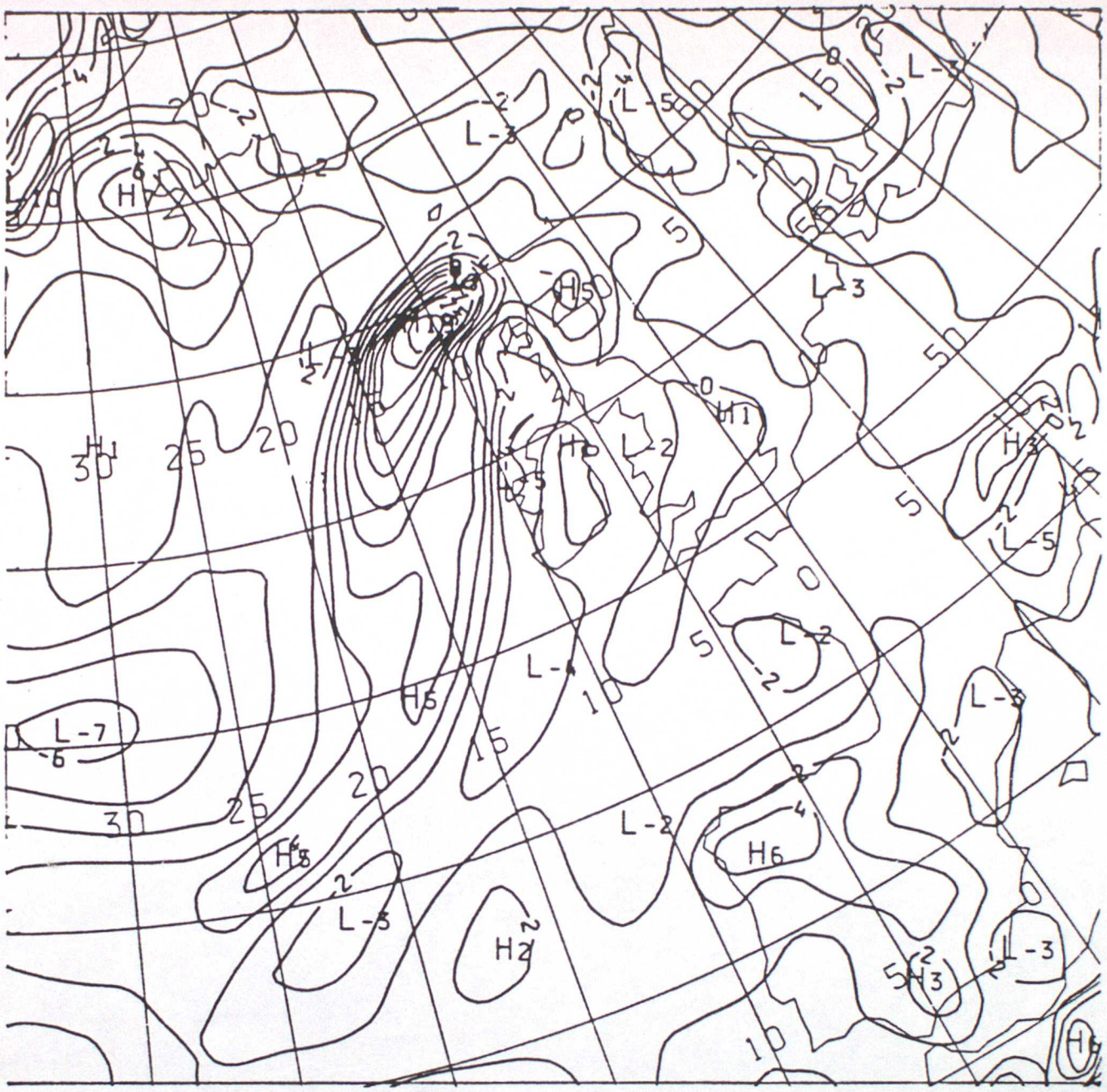

Fig. 7

Fig. 8

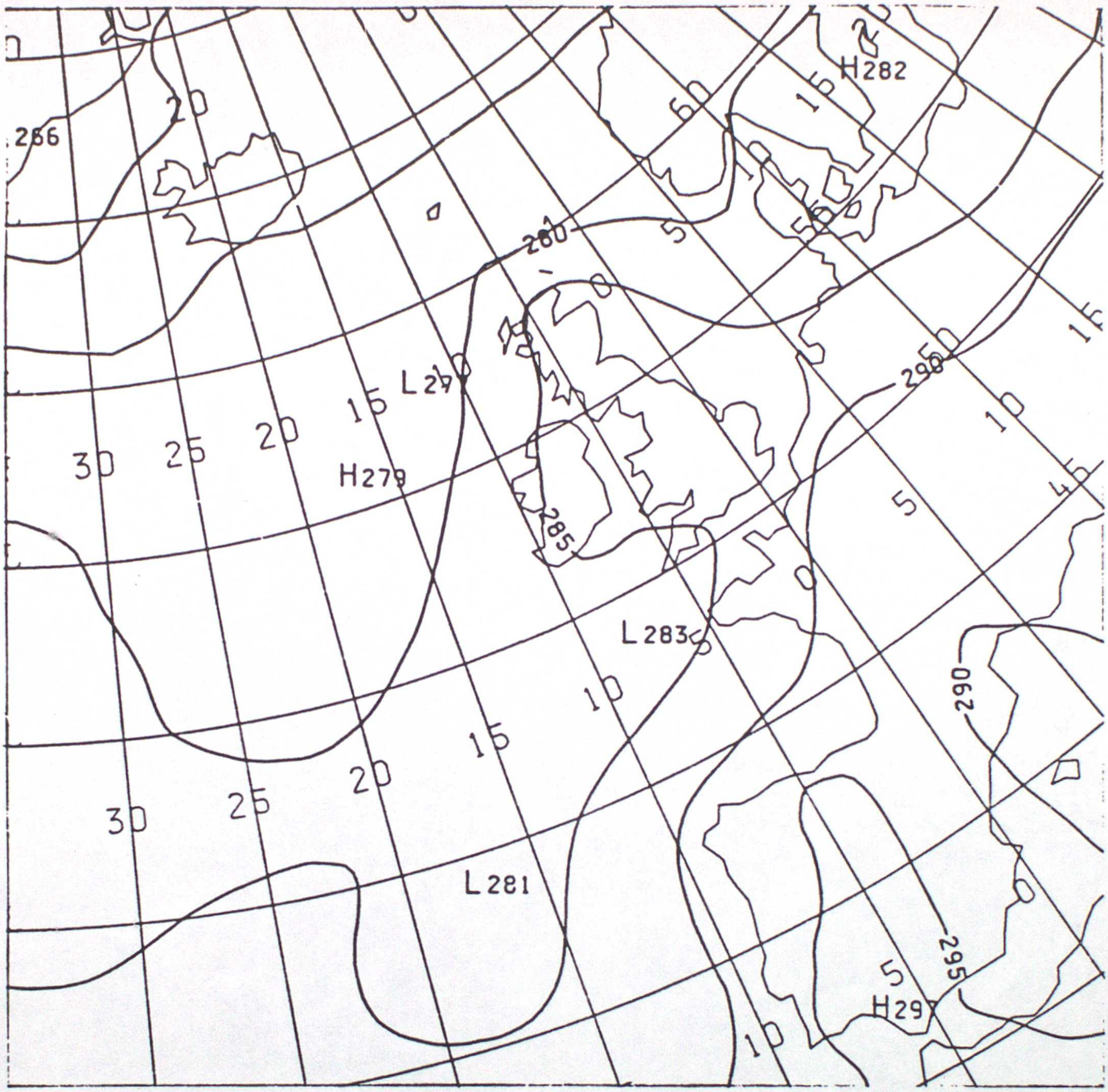

Fig. 9

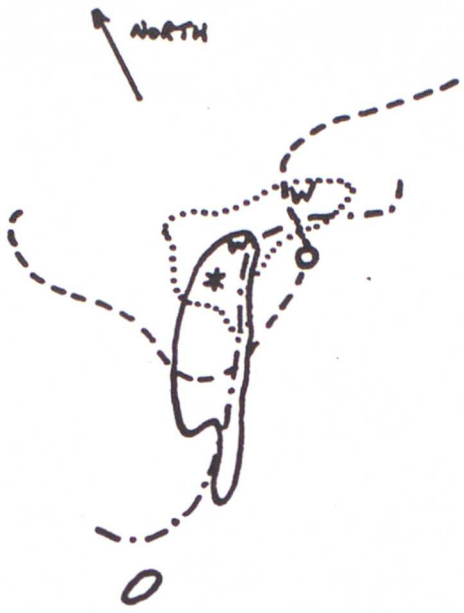

Key

——— 1000 mb vorticity = 4×10^{-5} s^{-1}

- - - - 1000 mb height = 60 m

—·—·— 900 - 1000 mb layer mean temperature = 280 K

..... 550 mb vertical velocity = $-4 \mu b$ s^{-1}

* Pressure centre and max vorticity

W Max ascent at 550 mb

Fig. 10

SIZE OF CROSS AT 950MB +

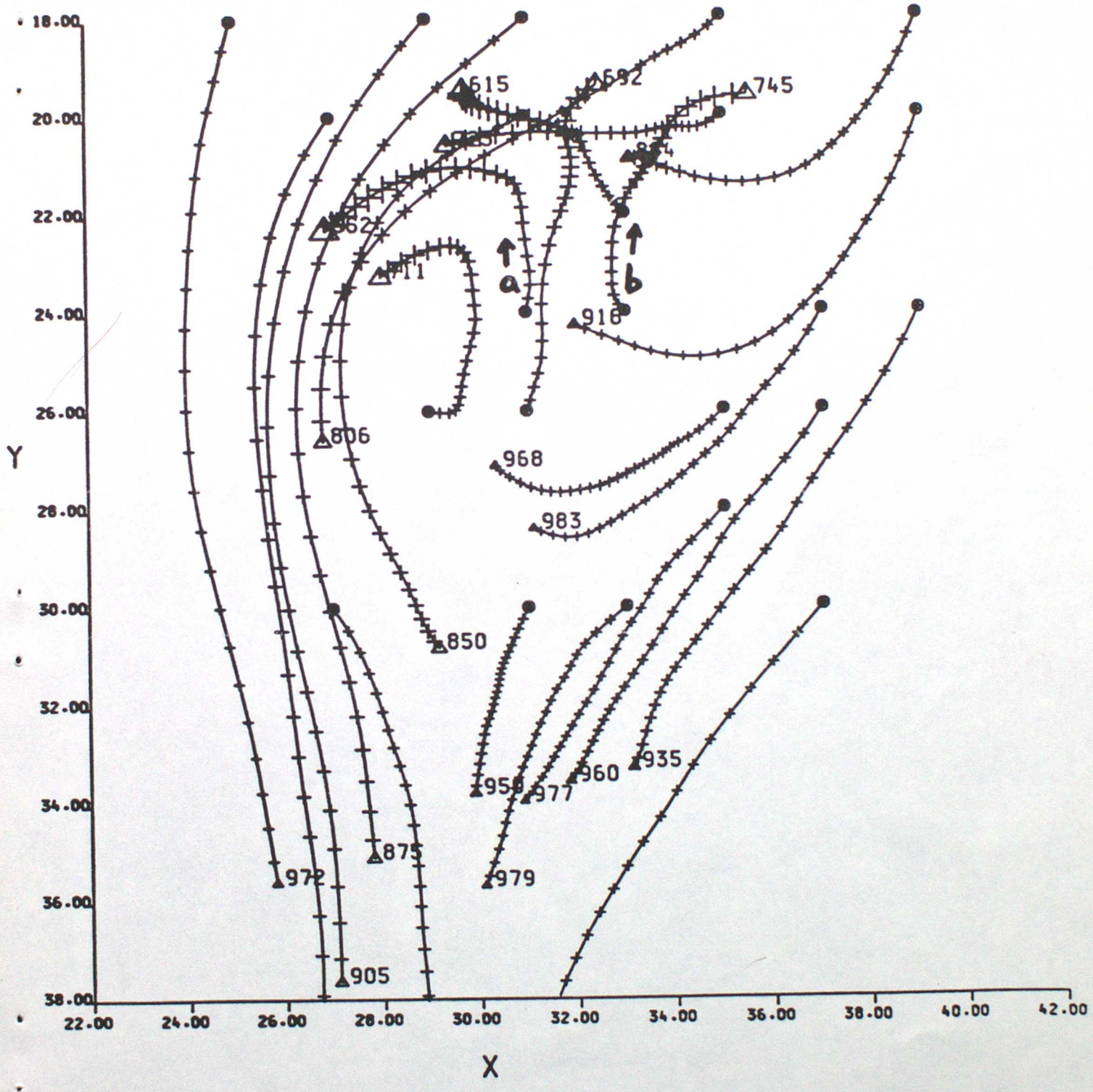

Fig. 11

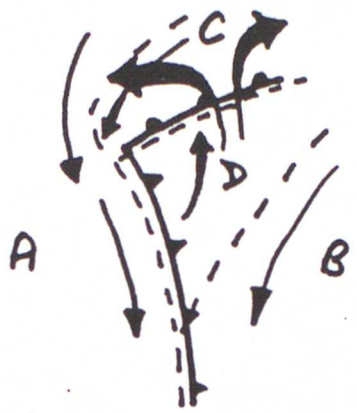

Fig. 12

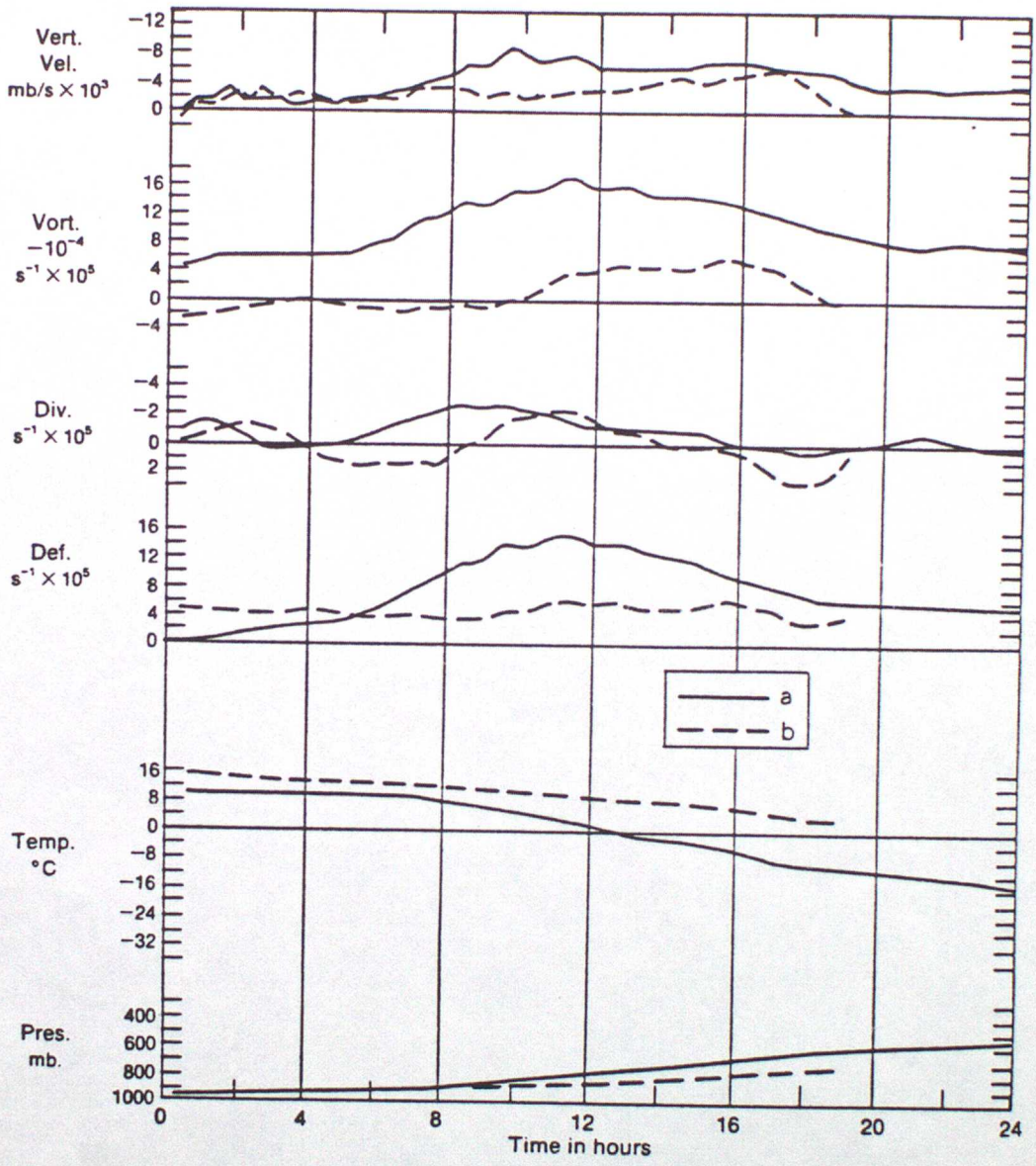
Vert. Vel. mb/s × 10³
−12
−8
−4
0
Vort. −10⁻⁴ s⁻¹ × 10⁵
16
12
8
4
0
−4
Div. s⁻¹ × 10⁵
−4
−2
0
2
Def. s⁻¹ × 10⁵
16
12
8
4
0
a
b
Temp. °C
16
8
0
−8
−16
−24
−32
Pres. mb.
400
600
800
1000
0
4
8
12
16
20
24
Time in hours

Fig. 13

SIZE OF CROSS AT 750MB +

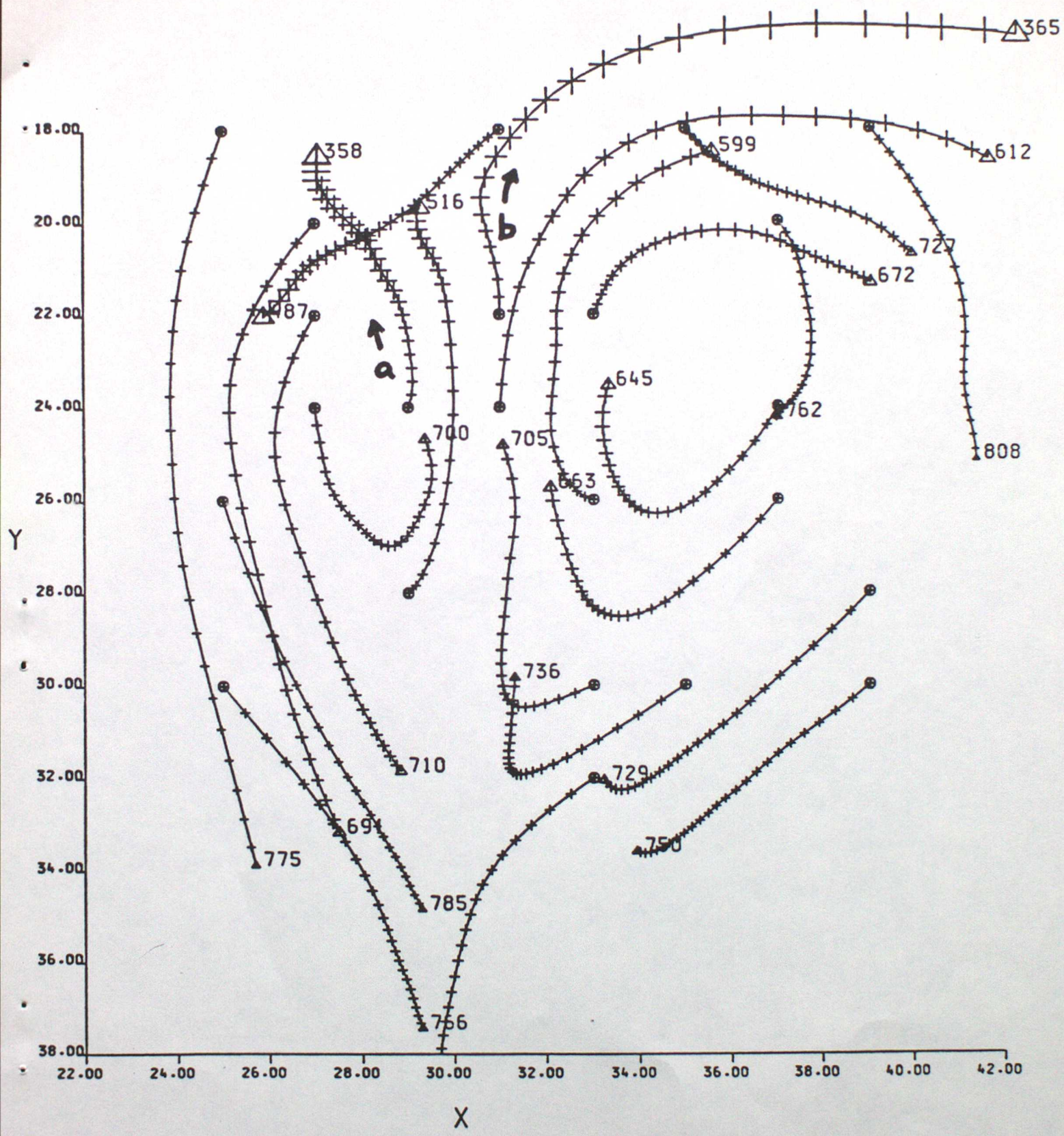

Fig. 14

Fig. 15

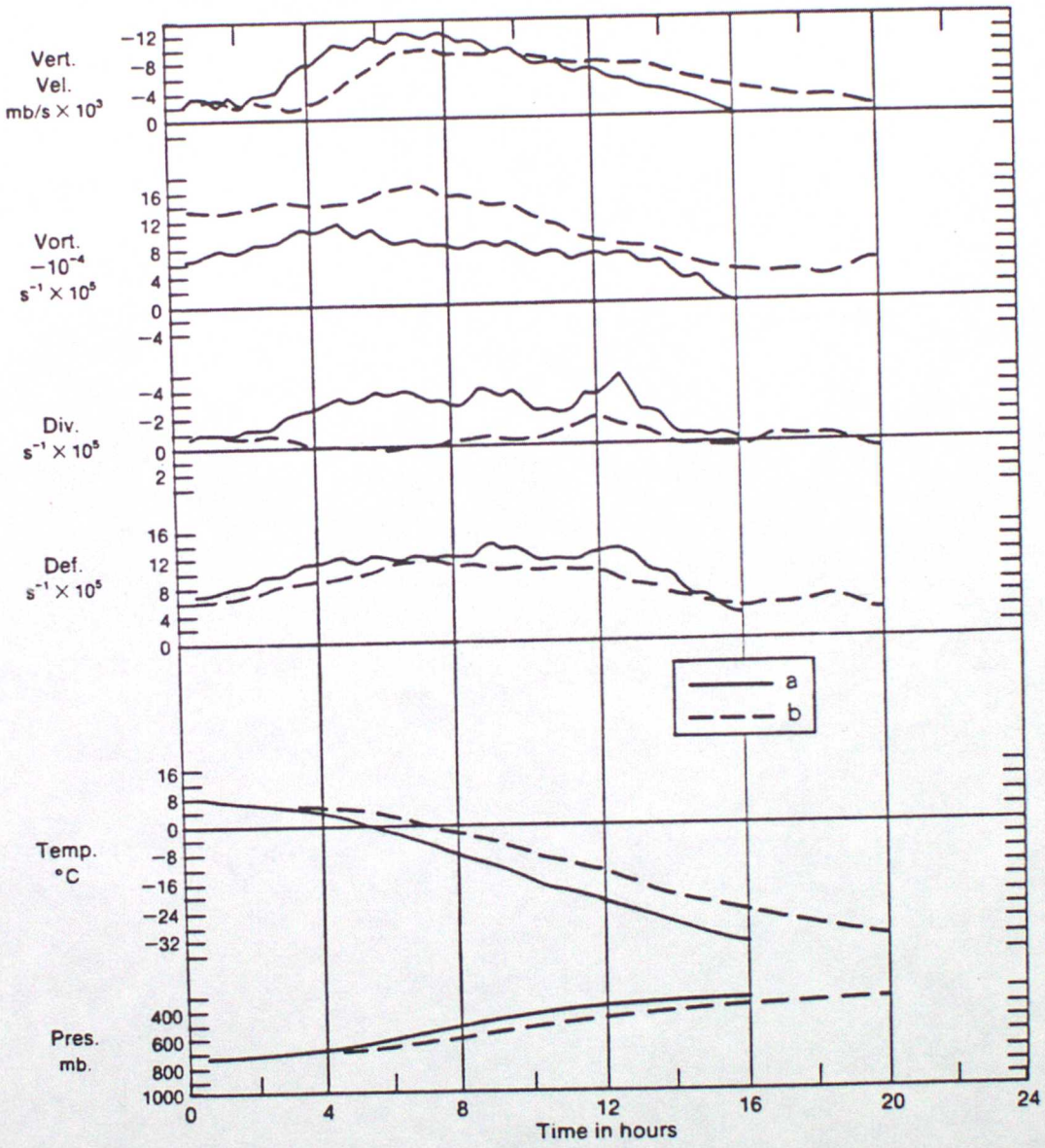
Vert. Vel. mb/s × 10³
−12
−8
−4
0
Vort. −10⁻⁴ s⁻¹ × 10⁵
16
12
8
4
0
−4
Div. s⁻¹ × 10⁵
−4
−2
0
2
Def. s⁻¹ × 10⁵
16
12
8
4
0
a
b
Temp. °C
16
8
0
−8
−16
−24
−32
Pres. mb.
400
600
800
1000
0
4
8
12
16
20
24
Time in hours

Fig. 16

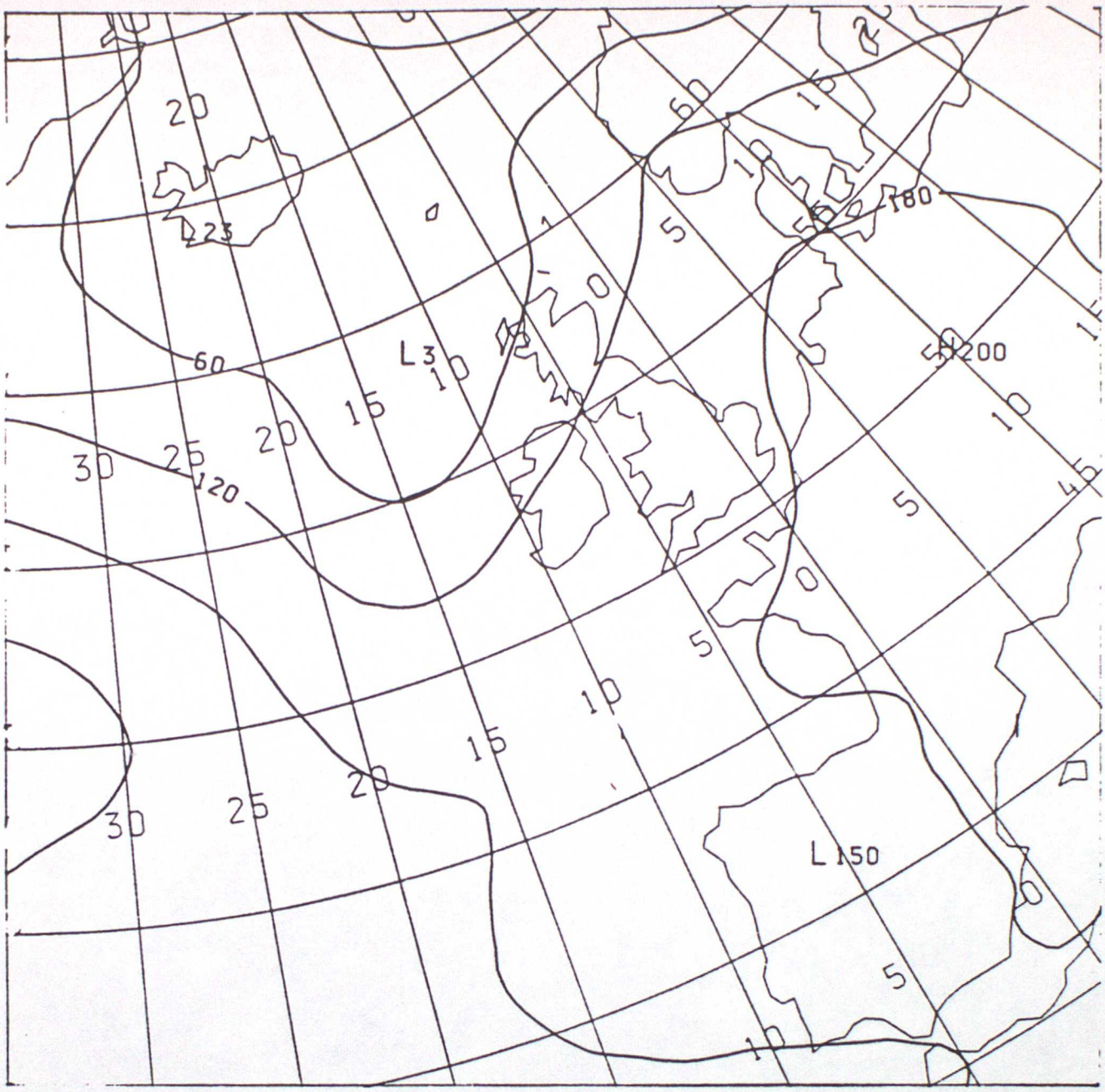

Fig. 17

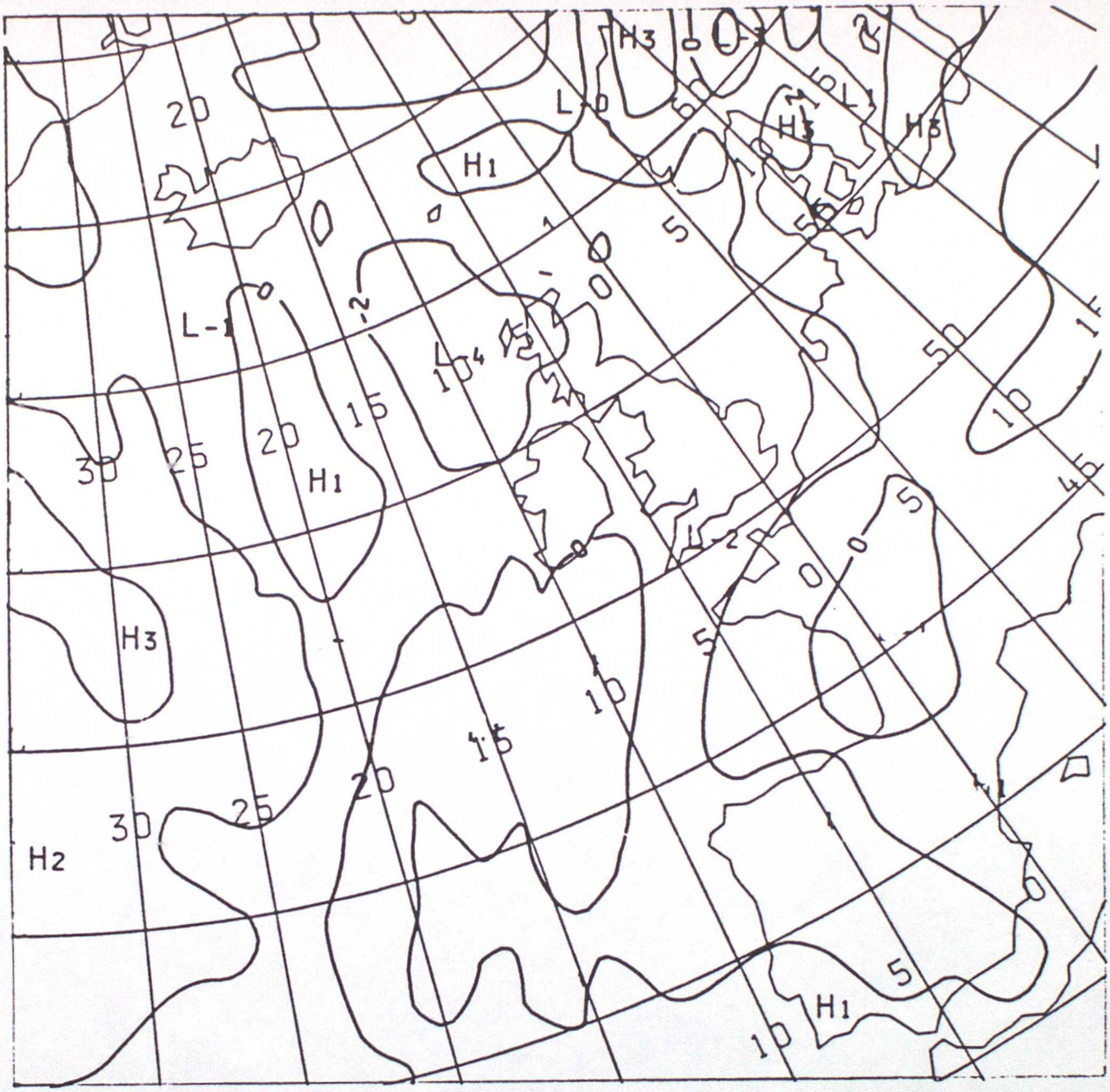

Fig. 18

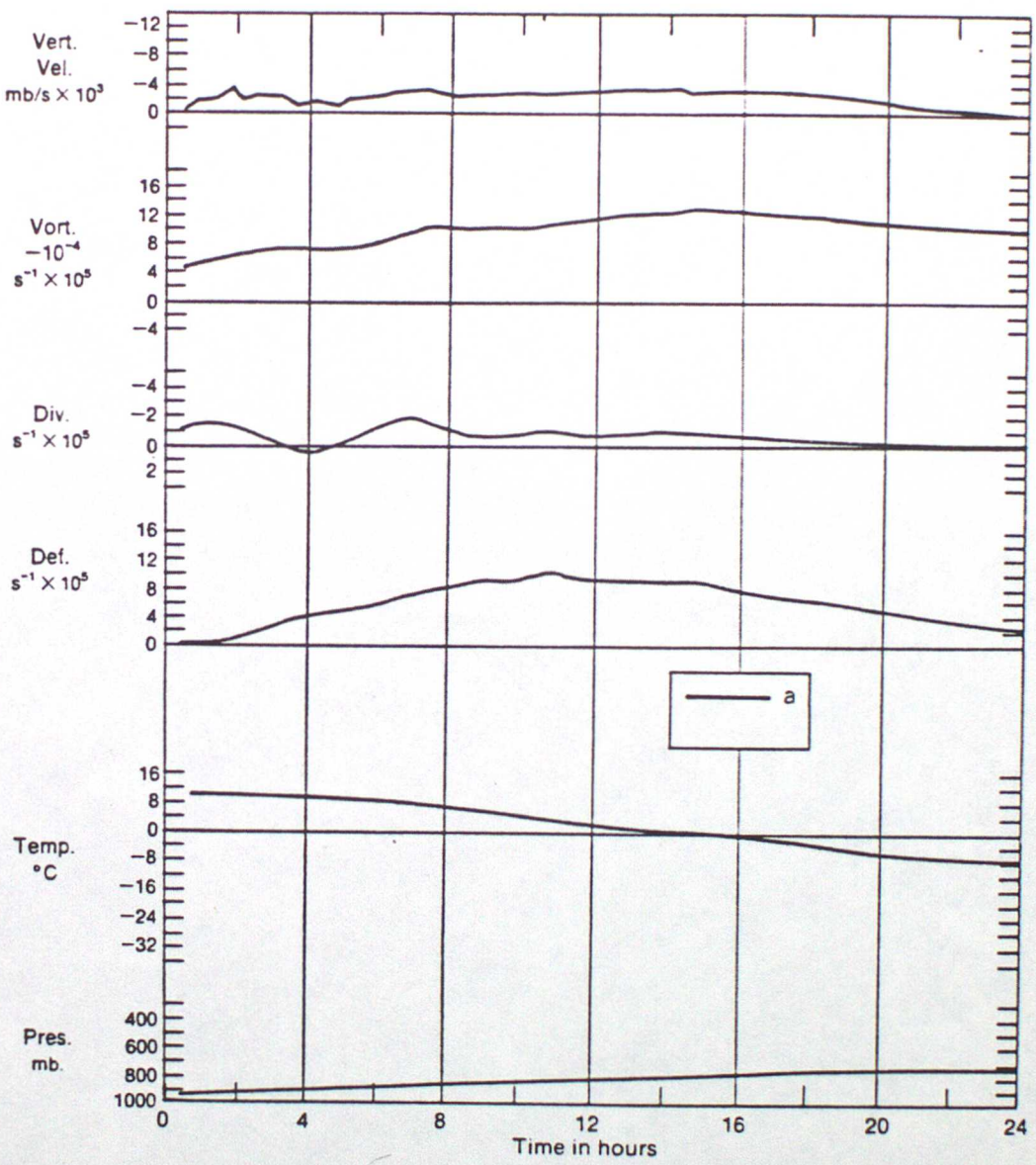
Vert. Vel. mb/s × 10³
−12
−8
−4
0
Vort. −10⁻⁴ s⁻¹ × 10⁵
16
12
8
4
0
−4
Div. s⁻¹ × 10⁵
−4
−2
0
2
Def. s⁻¹ × 10⁵
16
12
8
4
0
a
Temp. °C
16
8
0
−8
−16
−24
−32
Pres. mb.
400
600
800
1000
0
4
8
12
16
20
24
Time in hours

Fig 19

Fig. 20

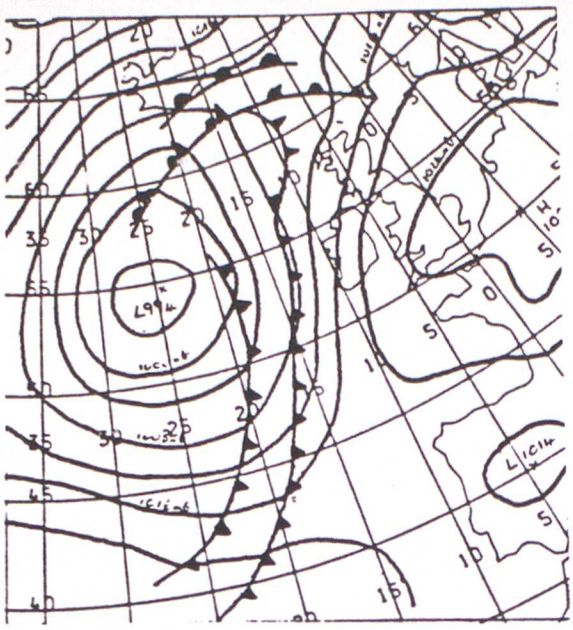

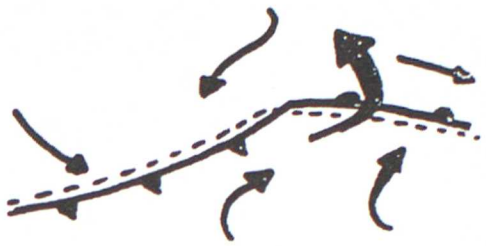

Fig. 21

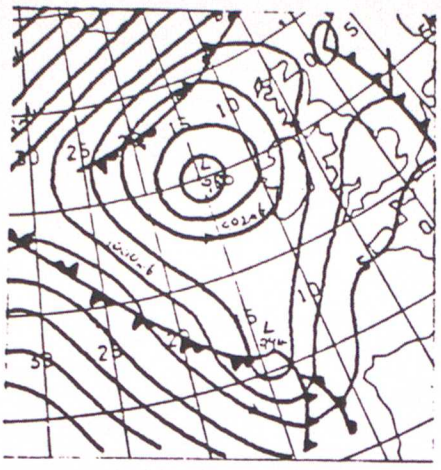

Fig. 22

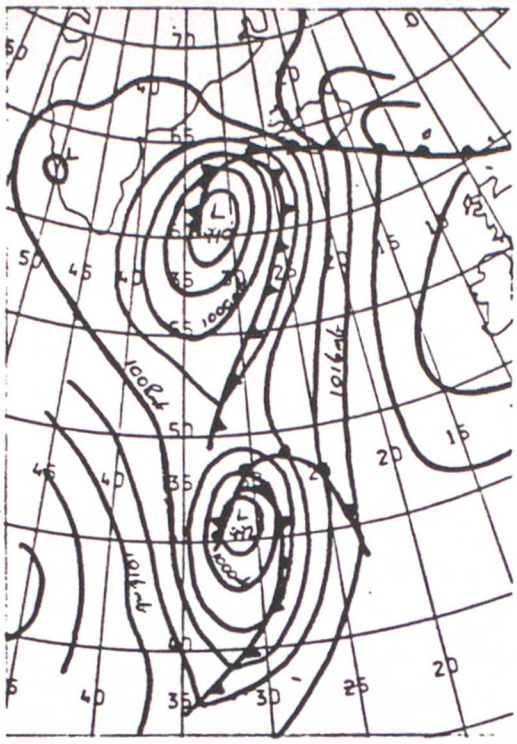

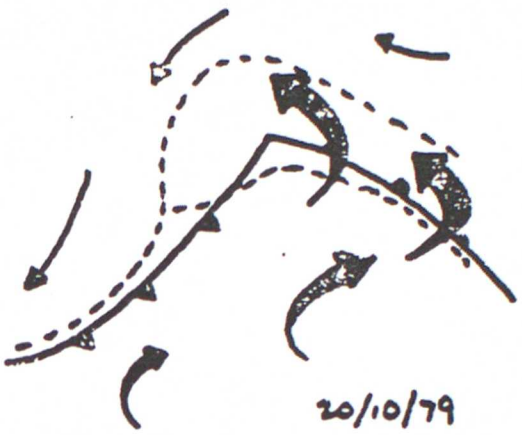

Fig. 23

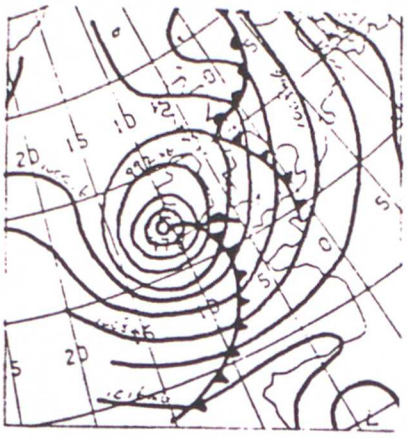

Fig. 24

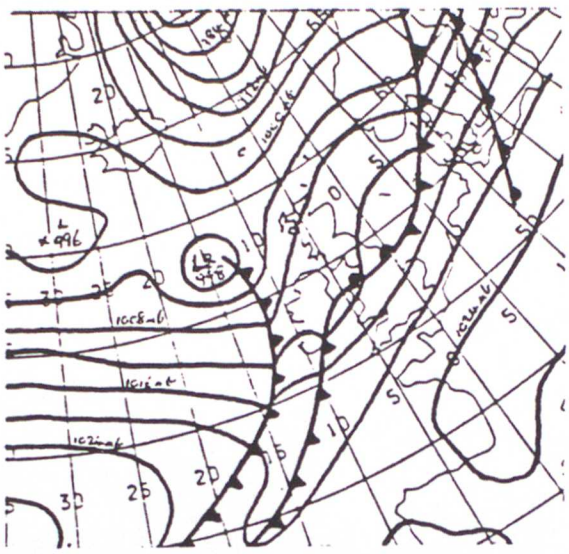

Fig. 25

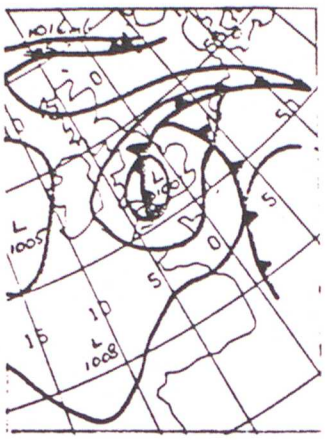

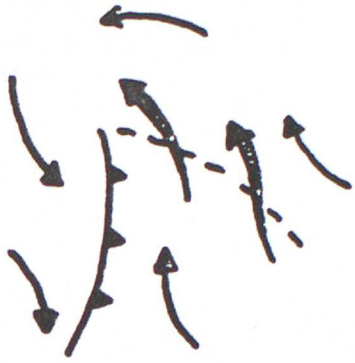

Fig. 26